Research of Pattern Formation, edited by R. Takaki, pp. 301–327.

Chemically Driven Dynamic Patterns at an Oil-Water Interface: Experimental Analysis of Nonlinear Waves and Oscillations

Shoichi KAI, Stefan C. MÜLLER*, Toshio MORI, and Mutsumaro MIKI

Department of Electrical Engineering, Kyushu Institute of Technology, Tobata. Kitakyushu 804, Japan

Abstract. An experimental investigation is presented of chemically driven dynamic instability of an oil-water interface in a cylindrical or annular glass container. The immiscible liquids are water containing a surfactant (TSAC) and nitrobenzene containing iodine. The reaction at the interface leads to complex deformation patterns including rotating solitary waves, multiple wave trains, periodic and non-periodic oscillations, source-to-sink propagation, and intermittent behavior. A phase diagram is established for the two solute concentrations ranging from 10^{-4} to 10^{-1} M. It shows 5 distinct regions of different dynamic regimes, determined by interaction of at least three mechanisms: dynamic wetting of the container wall, capillary effect, and Marangoni instability of the liquid-liquid interface. The influences of aspect ratio, concentration product, and temperature are investigated and local time traces are derived from electropotential differences. Their spectral analysis reveals details of periodic or irregular motion. Transitions between the dynamic modes of the system during its temporal evolution are recorded. Quantitatively determined profiles of regular waves are analyzed by exponential functions and a simple model for this is proposed.

1. Introduction

Spatial and temporal ordering on a macroscopic scale is a well studied phenomenon occurring in nonequilibrium physics and chemistry. The ordering

* Permanent address: Max-Planck-Institut für Ernährungsphysiologie, Rheinlanddamm 201, D-4600 Dortmund 1, FRG.

processes are governed by highly nonlinear interactions. Patterns arising from hydrodynamic instabilities, for instance, are frequently discussed in terms of mode selection, wave propagation, defect dynamics, or the influence of boundary conditions and container geometry (1, 2) and a wide variety of stationary, transient, chaotic or intermittent behavior is known. Much effort has been also devoted to understand similar structures in chemical systems such as the Belousov-Zhabotinskii reaction in which multistability, limit cycle behavior, chaos, and periodic spatio-temporal patterns, in particular travelling waves due to reaction -diffusion coupling are observed (3, 4). These phenomena have been treated theoretically in the framework of nonequilibrium thermodynamics (5).

In recent years, several authors (6–11) have investigated complex dynamic deformations of a liquid-liquid interface which occur when chemical reactions are coupled with hydrodynamic instabilities, as often observed in the chemical engineering field (12). Large-scale chemically driven motion of an interface between an organic and an aqueous solution was first shown in 1971 by Dupeyrat and coworkers (6) who further made salient contributions concerning the hydrodynamical and physicochemical effects leading to the instability (7). In this system a surfactant is dissolved in the aqueous phase and the interfacial tension is changed by reaction at the interface with a compound supplied from the organic phase. This results in pronounced dynamic interfacial deformations, e.g., several waves rotating along the container wall as shown in Fig. 1, soliton like behavior (13), or irregular nonperiodic motion. Mainly the temporal properties of this system were studied by Yoshikawa *et al.* (8) on the basis of electrical potential measurements, while a rough overview about spatiotemporal patterns and the different dynamic regimes of wave

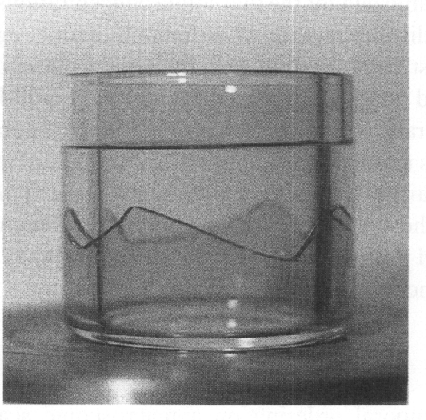

Fig. 1. Photograph of interfacial waves propagating in an annular container (outer diameter $\phi_1 = 50.3$ mm; spacing $d = 2.6$ mm; height $H = 50$ mm). Equal volumes (7 ml) of solutions A and B with concentration $c_A = 10^{-3}$ M and $c_B = 2 \times 10^{-3}$ M were poured into the space between the two cylindrical columns. The amplitude of the 4 waves is 10 mm.

propagation was given in (9, 10). If a small drop of the organic phase is submerged in a pool of aqueous medium it starts to rotate or to perform erratic motions. This led Sackmann to discuss the possible role of this chemomechanical energy conversion for locomotion of biological cells on solid substrates (11).

So far, no comprehensive theoretical picture has been developed yet. A stability theory for surface deformation due to a first order chemical reaction between gas and liquid was achieved by Sakata *et al.* (14), but the wave form and the motion after occurrence of the instability was not discussed in any detail. Recently, waves were analyzed by approximating convective flow near the interface by a Hele-Shaw cell and introducing a phenomenological equation for interfacial tension changes (15).

Since a comprehensive characterization of the entire dynamics of this system has not yet been reported we extended our previous work (9, 10) and investigated the interfacial system in more experimental detail. Our studies emphasize the large variety of phenomena induced by Marangoni instability of the interface due to changes in interfacial tension (16, 17). We distinguish between the "capillary effect" which is the up or downward displacement of the interface caused by interfacial forces in the gravitational field, interfacial turbulence due to a convective Marangoni instability, and changes of the contact angle due to variation of the wetting behavior of the liquid/solid interface at the boundary of the container (18). Furthermore, we note that there is an interesting analogy between the chemically driven patterns and those forming on the surface of a liquid in a container that is subjected to external mechanical vibrations: the so-called bell mode instability (19, 20).

In this article, we summarize our measurements of the dynamic features of interfacial instability. The following section describes preparation, container geometry and methods of investigation. In the result section, we give a classification of the most remarkable features of waves and oscillations and their spatial profiles on the basis of visual observation, complemented by local measurement of electrical potential difference. Time evolution of dynamic states for given initial conditions is followed in some detail. A number of spatial profiles can be quantitatively represented by exponentials. This mostly phenomenological survey is concluded by pointing to various mechanistic aspects with respect to the coupling between reaction and hydrodynamic and diffusive transport which will be treated in more detail in a subsequent publication (21, 22).

2. Experimental

2.1 Materials

The immiscible solvents were water and nitrobenzene. When placed in contact with each other, the two liquids form a well defined interface. The solutes were the surfactant trimethyl-stearyl-ammonium chloride (TSAC, $C_{18}H_{37}N(CH_3)_3Cl$) and iodine (I_2) (7). All chemicals were purchased from Tokyo Kasei Co. (best grade)

and used without further purification. Solutions were made by dissolving TSAC in water (aqueous phase A) and I_2 in nitrobenzene saturated with potassium iodide (organic phase B). About 120 combinations of concentrations of TSAC, c_A, and of iodine, c_B, were prepared, each concentration ranging from 10^{-4} to 10^{-1} M.

2.2 Containers and Sample Preparation

Interfacial patterns were investigated in two container geometries (Fig. 2): (1) cylindrical containers (beakers) with inner diameter ϕ; and (2) annular containers consisting of two concentric glass cylinders (diameters ϕ_1, ϕ_2) sealed to a bottom plate and separated by a ring-shaped gap (spacing d). The vessels used in the experiments are listed in the Table 1.

A volume of solution B (typically 2.7 ml for a cylindrical container with ϕ =

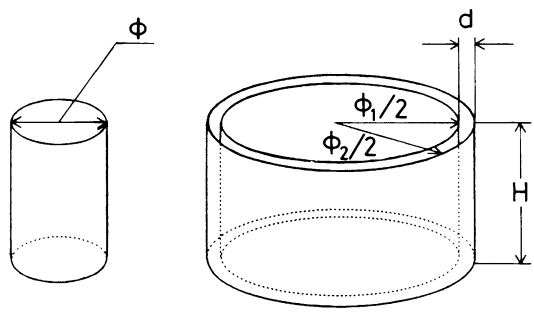

Fig. 2. Schematic drawings of the containers: (a) Cylindrical glass vessel (beaker) with inside diameter ϕ. (b) Annular container consisting of two concentric columns sealed to a bottom plate; ϕ_1 is the outer diameter of the smaller, ϕ_2 the inner diameter of the larger column, *d* the thickness (spacing) of the annulus. *H* is the heights of the containers.

Table 1. Containers for the experiments. The solution volumes *V* for the annular containers are specified, those for the cylindrical containers can be calculated from the aspect ratios. ϕ: cylindirical container, ϕ_1, ϕ_2, *d*, V: annular container.

cylindrical container	annular container			
ϕ (mm)	ϕ_1 (mm)	ϕ_2 (mm)	*d* (mm)	*V* (ml)
10, 13	80.0	75.2	2.4	10
15, 16	80.0	70.0	5.0	20
19, 24	50.3	45.1	2.6	7
28, 32	50.4	39.6	5.4	10
	31.1	25.1	3.0	6
	31.2	20.4	5.4	9

19 mm) is first placed into the vessel, then an equal volume of solution A is poured on top of the organic phase. Due to its higher density ($\rho_B = 1.35$ g/cm^3) solution B always occupies the lower part of the vessel, while solution A ($\rho_A = 1.0$ g/cm^3) stays on top. Upon contact between the solutions, a chemical reaction starts that produces $C_{18}H_{37}(NH_3)_3I$. In the course of time this product becomes weakly visible as a yellow precipitate at the interface. Immediately after the start, the contact area is distorted, indicating the onset of interfacial instability. For instance, in a beaker with $\phi = 19$ mm and $c_A = c_B = 10^{-3}$ M waves with an amplitude of 10 mm start to propagate along the wall at a velocity of 13 cm/s, corresponding to an angular velocity of 14 rad/s (similar to the example for an annulus shown in Fig. 1). Samples were prepared for 8 values of ϕ (see Table 1) with varying aspect ratio $r = \phi/\delta$, where δ is the solution depth between bottom and interface.

For starting an experiment in an annulus (see Table 1) the liquids were poured into the gap between inner and outer cylinder. In this arrangement, the interfacial motion is more distinct and a larger variety of dynamic features is observed as compared to the beakers. A special container was used for electric potential measurements, as specified in Subsection 2.3.

All experiments were performed at 24°C unless stated otherwise. The temperature was controlled within ±1°C.

2.3 Methods

The surface tension of the solutions, γ, was measured with the capillary method, the specific conductivity, σ, with a universal bridge (Yokokawa Electric Corp. BV-Z-13A) at 1 kHz using several concentric electrode cells.

The dynamic behavior of the interface and its temporal evolution was visually observed and classified as a function of several system parameters: mainly the concentrations c_A, c_B, the container geometry (aspect ratio r, diameters), and the temperature T. Measured quantities were the number of waves, n, the wave amplitude, h, the propagation velocity, v, (or rotation frequency, ω), and the lifetime, τ, of a dynamical state. Wave forms and profiles were described qualitatively and also recorded with a TV camera (Panasonic VY51) linked to a video tape recorder (JVC BR-8600) and a video signal processor (ADS Co. PIP-4000) linked to a personal computer (NEC, PC9801) by special interface circuits.

For several cases of waves in an annulus, the video images were further analyzed in two ways: (1) The wave profiles are copied directly from a snapshot displayed on the TV monitor. No correction was made to account for the distortions at the container edges due to the projection of the circular vessel geometry on the screen. (2) For quantitative discussion, a procedure was used which applies only to wave profiles that do not change during rotation: along a vertical line at the container center (resolution 480 pixels) intensity profiles were recorded at a rate of 30 lines/s. From their temporal change and by using the measured value of the propagation velocity, a spatial profile was reconstructed.

For measuring the spatial and temporal variation of ion concentration close to

the interface, a special cylindrical container was equipped with platinum point electrodes (diameter, 0.5 mm). One electrode was positioned just at the interface at middle height of the vessel, the other in the bulk of the aqueous phase far away from the interface. The potential difference, $\Delta\psi$, was recorded with a pen recorder (Panasonic VP6541A) and stored on magnetic disk for further processing and simultaneously analyzed with a signal FFT analyzer (Iwatsu SM-2100). Since the electrode system was not calibrated with respect to a standard potential and no ion-selective electrodes were used, only relative variations of $\Delta\psi$ were detected.

3. Results

3.1 Surface tension and electric conductivity

Surface tension, specific conductivity, and density of the solutions are relevant physico-chemical quantities that influence the dynamic behavior of the interface. In the range from 3×10^{-5} to 10^{-1} M the surface tension of the aqueous phase depends on the TSAC concentration according to the empirical relation (10)

$$\gamma_A[\text{dyne / cm}] = \frac{9.3}{\log(c_A / 2 + 1) + 0.2} + 28$$

where c_A is given in units of 10^{-5} M, whereas the surface tension of the organic phase, γ_B, has a constant value of 46 dyne/cm within a few percent. Both surface tensions are equal near 4×10^{-5} M. Thus, for concentrations above this value the initial γ_A is always smaller than γ_B, but with sufficiently decreasing c_A it becomes larger. The contact angle α of the interface at the solid container wall is determined by the interfacial tensions γ_{OG}, γ_{WG}, and γ_{WO} (see Fig. 3) according to

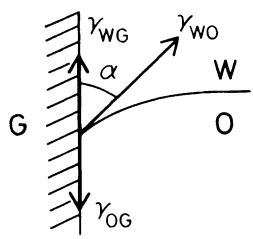

Fig. 3. Contact angle α between the glass wall of the container and the oil/water interface. The vectors of the equilibrium interfacial tensions between oil and glass (γ_{OG}), water and glass (γ_{WG}), water and oil (γ_{WO}),are indicated.

$$\cos\alpha = \frac{\gamma_{OG} - \gamma_{WG}}{\gamma_{WO}}$$

Assuming that $\gamma_A \approx \gamma_{WG}$ and $\gamma_B \approx \gamma_{OG}$, changes of concentration clearly affect the contact angle, especially if by lowering the surfactant concentration the interfacial tensions become close to each other (around 4×10^{-5} M) which may easily induce transitions between $\alpha > 90°$ and $\alpha < 90°$. This change, however, is a quite local phenomenon and happens only near the glass surface. The main influence of interfacial tension is attributed to its effect on capillary forces. In this system the difference $\Delta\gamma = \gamma_A - \gamma_B$ is taken as a measure of these forces at the interface. The absolute value of $\Delta\gamma$ is in the same range as measured directly in (7).

The specific conductivities σ_A, σ_B are linear functions of the concentrations c_A, c_B in the investigated concentration ranges. The slope of σ_A is slightly larger than that of σ_B, and the two lines intersect at $c_A = c_B = 10^{-2}$ M, indicating that, under the condition $c_A = c_B$, $\sigma_A > \sigma_B$ when both concentrations are smaller and $\sigma_A < \sigma_B$ when they are larger than this value.

There is a substantial difference between the densities of the two phases ($\rho_A - \rho_B = 0.35$ g/cm^3). In the gravitational field, this is of importance for the degree of vertical displacement of the unstable interface.

3.2 Dynamical features of interfacial motion

3.2.1 Classification of waves, periodic and non-periodic motion

The interfacial system exhibits a complex variety of structural and dynamical features. As evident from simple visual observation there occur macroscopic dynamic phenomena such as solitary waves of different shapes (13), multiple rotating wave trains (already shown in Fig. 1) with constant or variable number of waves, periodic and non-periodic oscillatory deformations that do not rotate, steady source-to-sink propagation, splitting and recombination of waves (9). As an additional example we show in Fig. 4 the propagation of a solitary wave as observed on a TV screen. Its profile is of the relaxation oscillation type and remains unchanged during rotation.

The details of the interfacial dynamics always depend sensitively on the initial and boundary conditions of the experiments, e.g., on factors such as temperature control, solution depth, container curvature, or surface properties of the glass wall. In this section, we characterize the dynamic behavior found in cylindrical containers with aspect ratio $r = 0.44$ at room temperature. This system shows qualitatively all the features that are characteristic for a wide range of experimental conditions.

The waves moving along the boundary of the container have characteristic profiles. Examples for periodically rotating waves are shown schematically in Fig. 5: among them solitary waves (solitons and anti-solitons), cusps, kink-waves, and more complex shapes. These are always highly asymmetric which points to the nonlinear character of the underlying processes in that the interfacial instability

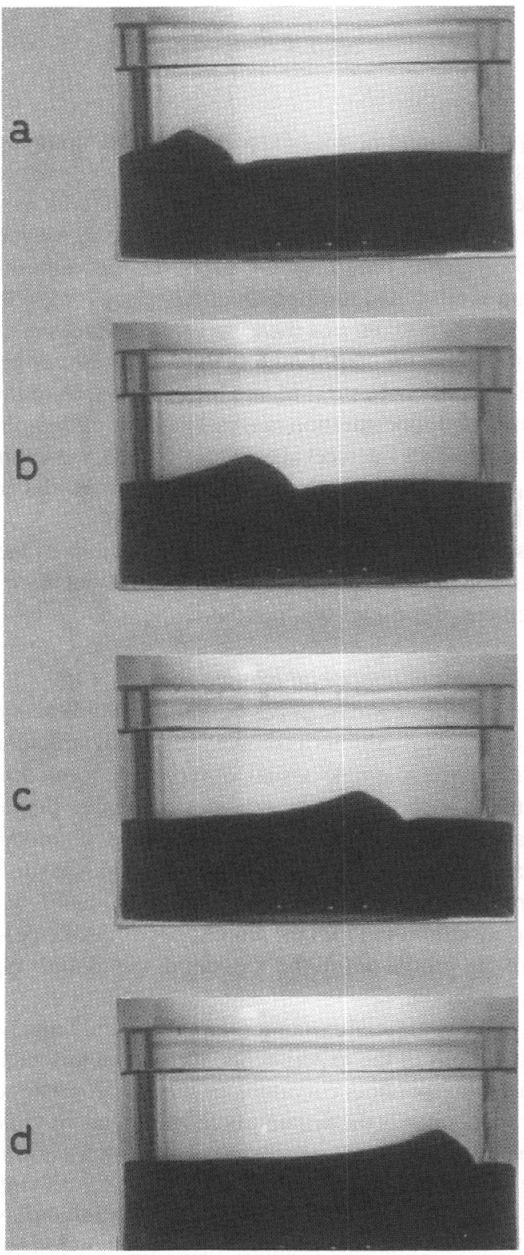

Fig. 4. A solitary wave with relaxation-type profile propagates in the gap of an annular container ($\phi_1 = 85$ mm, $\phi_2 = 80.4$ mm) with $c_A = 10^{-2}$ M and $c_B = 3 \times 10^{-2}$ M at $T = 26°C$, as photographed from a video screen. Time interval between successive snapshots is 1/15 s.

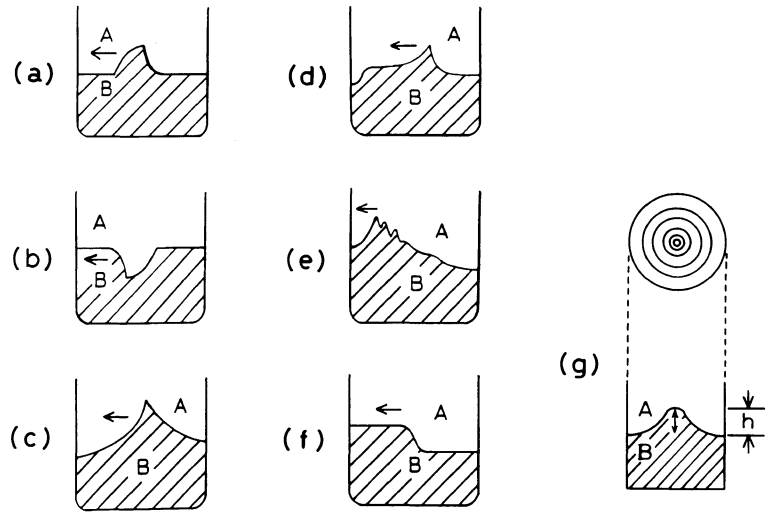

Fig. 5. Schematic profiles of wave-like deformations of the interface between aqueous (A) and organic phase (B) in a cylindrical container: (a) solitary wave (soliton), (b) antisoliton, (c) cusp wave, (d) cusp wave with plateau, (e) wave with secondary wiggles, and (f) kink-like wave. Arrows indicate direction of motion. In (g) a periodic isotropic stretching motion of the interface is illustrated from above (contour lines) and from the side (profile).

occurs not only for one elementary frequency but involves a complex spectrum of higher harmonics. In a top view of the container we give in Fig. 6 several examples of multiple wave trains. They can be arranged in a symmetric fashion (see Fig. 6a–c, up to sixfold observed) or follow each other in an irregular but steadily maintained angular sequence (Fig. 6d). A non-periodic case is illustrated in Fig. 6f where wave crests have different angular velocities and may overtake each other.

Some specific features of the rotating or oscillatory macroscopic deformations, strongly dependent on the precise experimental conditions, are the following (10):

(1) Solitary waves moving in opposite direction often disappear upon collision, or a larger wave may absorb a smaller one. Depending on the type (profile) of wave they may also pass through each other as solitons in conservative systems commonly do (compare Fig. 18 below).

(2) Steady wave propagation between a source and a sink at stationary locations is frequently produced (Fig. 6e). At the source, a pair of waves emerges with opposite angular momentum disappearing by collision in the sink on the opposite side of the container. This behavior is preferentially observed in the boundary region between regions I and II of the phase diagram (see Fig. 11), and especially in annular container geometries with not perfectly coaxial wall ar-

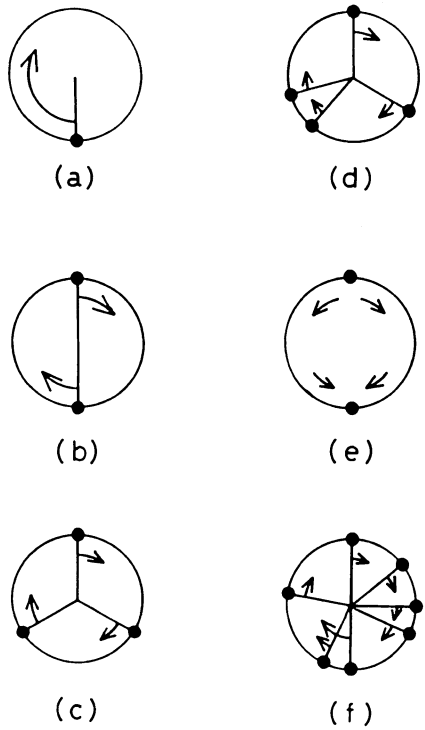

Fig. 6. Schematic top view of multiple waves in a cylindrical container. Black dots indicate position of wave crests at the container wall. The angle between subsequent crests in (a) to (c) is 2π (solitary wave), π, $2\pi/3$, respectively. In (d) angles are incommensurate but are steadily maintained. In (e) waves travel between source and sink (black dots), (f) shows a complex (chaotic) and unsteady wave train.

rangement.

(3) Waves with different amplitudes frequently tend to split or recombine, thus producing new waves with sharper or flatter profiles (compare Fig. 17).

(4) Some waves travel with secondary wiggles on their shoulders that may move like secondary waves or just oscillate rapidly (cf. Fig. 5e).

(5) An isotropic stretching motion may take place from the center to the boundary and vice versa (cf. Fig. 5g); as well as oscillations (without rotation) between stationary locations at opposite ends of the container.

(6) In addition to steady or unsteady rotation or periodic and non-periodic oscillation, interfacial deformation may occur by drastic, intermittent bursts.

3.2.2 Electrochemical potential difference

Measurements of the electrochemical potential difference, $\Delta\psi$, offer a more quantitative analytical tool to distinguish between different modes of interfacial

motion (compare (8, 10)). Amplitude and width of the electropotential peaks are closely correlated with amplitude and width of waves passing the electrode location. Figure 7 shows a typical time trace of $\Delta\psi$ with peak to peak amplitudes of about 0.2 V. (At some concentrations $\Delta\psi$ reaches 0.6 V). For more than 12 min a regular, periodic regime with slowly changing period and shape prevails. After 15 min more irregular behavior sets in which, in this particular experiment, indicates that the pattern will disappear soon.

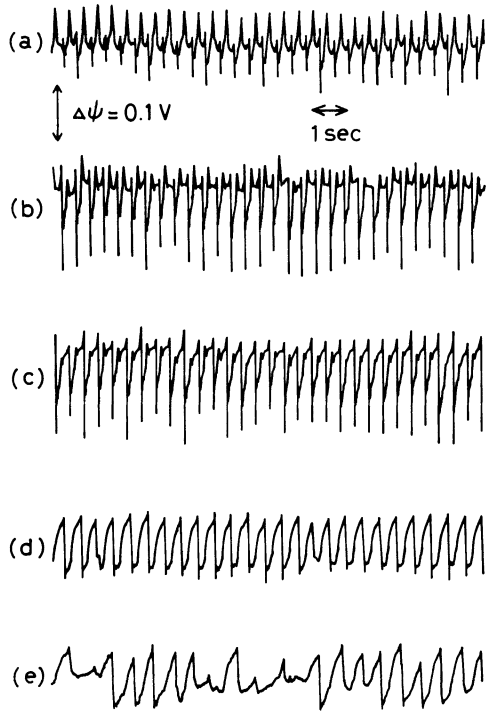

Fig. 7. Oscillations of electrochemical potential difference, $\Delta\psi$, between phases A and B, measured in a cylindrical vessel ($\phi = 19$ mm, $r = 0.44$) with $c_A = c_B = 5 \times 10^{-3}$ M. The time traces begin 38 s (a), 175 s (b), 275 s (c), 750 s (d), and 950 s (e) after the start of the experiment. With enhanced time resolution, curve (b) shows several peaks per period (see Ref. (10)).

Generally, it depends on the initial choice of concentrations what the predominant characteristics of these traces are during the most active phase of the interfacial motion (roughly the first 5 to 10 min): strictly periodic, periodic with superposed noise, or highly non-periodic. This is exemplified in Figs. 8 to 10: The power spectrum of the signal in Fig. 8a clearly consists of sharp peaks at one fundamental

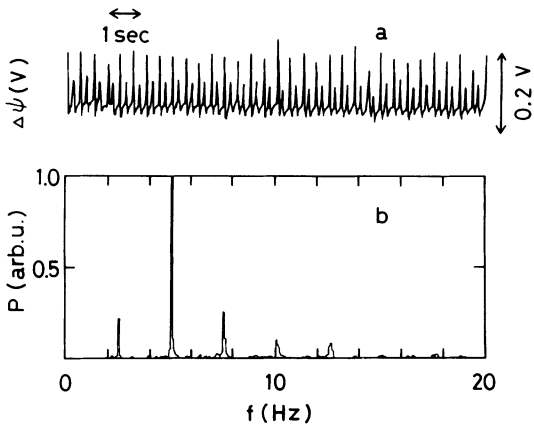

Fig. 8. (a) Periodic signal of $\Delta\psi$, obtained in a cylindrical container ($\phi = 19$ mm, $r = 0.44$) with $c_A = c_B = 2 \times 10^{-3}$ M at $T = 22°C$, (b) corresponding power spectrum (linear scale).

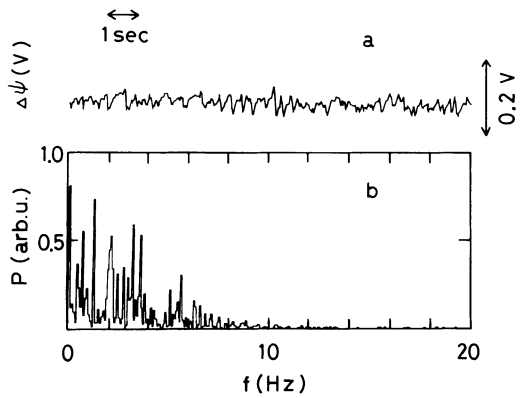

Fig. 9. Noisy signal of $\Delta\psi$ and its power spectrum (linear scale), obtained after 210 s in a container as in Fig. 8, with $c_A = c_B = 5 \times 10^{-3}$ M at $T = 30°C$. The macroscopic motion exhibits steady periodicity.

frequency and its harmonics. Interestingly, the apparently quite irregular signal depicted in Fig. 9a contains in its spectrum one very pronounced frequency combined with a number of widely distributed small-amplitude peaks, indicating that we encounter here a dynamic regime in which a basically periodic motion clearly possesses some noisy components. By contrast, the spectrum of the irregular signal in Fig. 10 is broadly distributed over at least one frequency decade.

Referring to the phase diagram of Fig. 11 below, clear periodicity is mostly

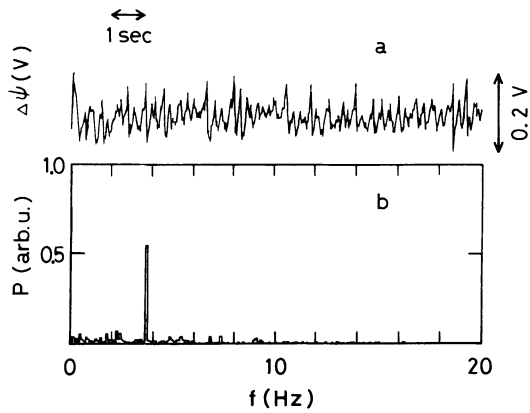

Fig. 10. As Fig. 8, but for a nonperiodic signal obtained with $c_A = c_B = 3 \times 10^{-2}$ M.

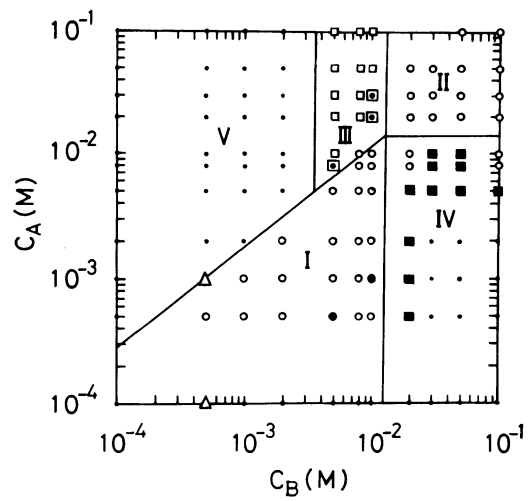

Fig. 11. Phase diagram of interfacial motions in the concentration plane (c_A: surfactant concentration in water, c_B: iodine concentration in nitrobenzene) for a cylindrical vessel ($\phi = 19$ mm, $r = 0.44$, $T = 24$°C). Details are given in the text.

found in region I, noisy periodic signals in region II, non-periodic irregular time traces in the high concentration part of II. It is noteworthy that convective flow on the surface (interfacial turbulence) could be clearly observed for the highest concentrations in region II, but not in region I. This points to the influence of different mechanisms as discussed in Section 4.

3.2.3 Phase diagram

From a large number of visual observations and potential measurements, we established phase diagrams in the (c_A, c_B)-plane for cylindrical containers with varying diameter and aspect ratio. In Fig. 11 such a diagram is shown for $\phi = 19$ mm and $r = 0.44$. The characteristic features of this diagram are the same for all r and 10.5 mm $< \phi <$ 24 mm, and life time, amplitude, velocity, temporal evolution and temperature dependence of the motions change only little. (Significant differences were observed for $\phi < 5$ mm.) For annular containers, too, we find essentially the same behavior.

The qualitative distinctions made in the diagram are based on the most typical, rather stable intermediate regime at the given concentrations, whereas other regimes that may appear during an induction or break-down period are disregarded. Thus, we distinguish between five regions (Fig. 11) for which different types of motion are characterized. In regions I and II most of the steady periodic motions take place including solitons, multiple waves, and oscillations with pronounced amplitude (symbol ○). Steady non-periodic (chaotic) motion can appear in region II, especially for the highest concentrations. Source-to-sink propagation (cf. Fig. 6e) is mostly observed in an annulus with small spacing in the boundary region between I and II. In the lower part of region I the wave rotation may become somewhat unsteady (symbol Δ) or lose its continuity which leads to intermittent bursts of active motion (symbol ●). In region III we frequently find the isotropic stretching motion (symbol , see Fig. 5g), and in region IV non-periodic motion with relatively small amplitude (symbol ■). Finally, in regions IV and V there are many cases in which no macroscopic motion can be detected (symbol ·), but in both regions the formation of a microemulsion at the interface forming small scale, irregular flow patterns can be readily observed under the microscope.

One phase boundary almost coincides with the diagonal in the concentration plane. In this context we note an important property of the shape of the interface: after the reaction finishes, the interface must remain concave with respect to the organic phase if $c_A < c_B$ and concave with respect to the aqueous phase if $c_A > c_B$. This follows from the numerical values for the concentration dependence of γ_A and γ_B (see Subsection 3.1).

Some general differences between regions I and II may be related to the difference between an oil-water and an water-oil emulsion. This is suggested by the fact that in I the organic liquid is pulled down along the container wall when a wave passes, while in II it is lifted up into the aqueous phase. Remarkably, for the conductivities $\sigma_A > \sigma_B$ holds for a large portion of region I, $\sigma_A < \sigma_B$ for a large portion of region II, and this relation is certainly fulfilled along the diagonal (see Subsection 3.1). This indicates that the ionic environment of the interface is an important factor for the macroscopic dynamics. In fact, the positive peaks in the $\Delta\psi$-signals occur in region I at the top of the actual wave form, but in region II they occur in the valley. Further results regarding electric field effects will be reported elsewhere.

Motions with relatively long lifetimes τ are found along the diagonal, those with the longest ($\tau > 15$ min) for concentrations $c_A = c_B$ ranging between 5×10^{-3} and 9×10^{-2} M (cf. Fig. 14). Furthermore, we note that the dependence of the lifetime on the temperature is opposite in regions I and II: in I, τ increases linearly, in II, τ decreases approximately exponentially with T.

3.2.4 Influence of concentration product and aspect ratio

The investigations of the phase diagram showed quite generally that for fixed geometry and temperature the motion becomes more active with increasing concentration product $c_A c_B$, i.e., oscillations get quicker, waves rotate faster and have larger amplitudes. This product can, in fact, be taken as a good representation of the thermodynamic driving force of the phenomenon. For cases of steadily rotating waves, we measured its influence on the maximum values of the rotation frequency ω_{max} and the amplitude h_{max} and show the results in Fig. 12. From the semilogarithmic plot in this figure the approximate relation is derived:

$$\omega_{max} \approx 0.44 \log(c_A c_B) + 3.24.$$

By linear extrapolation we obtain $\omega_{max} = 0$ for $c_A c_B = 4.4 \times 10^{-8}\,M^{-2}$, thus it is unlikely that any rotation takes place below this value. The above equation points to the

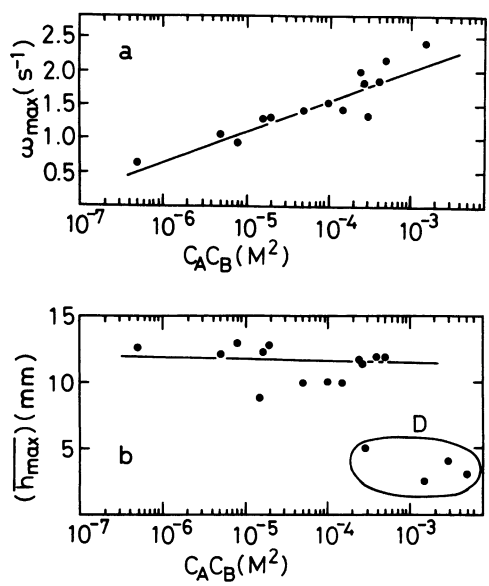

Fig. 12. (a) Maximum rotation frequency, ω_{max}, and (b) maximum amplitude, h_{max},, as a function of the concentration product $c_A c_B$ in a cylindrical vessel ($\phi = 16$ mm, $r = 0.625$).

relationship between the reaction kinetics and the speed of wave propagation (see discussion).

On the other hand, the maximum amplitude h_{max} does not significantly depend on $c_A c_B$ as long as relatively steady rotation and/or oscillations are considered (Fig. 12b). (The values in region D of the graph belong to random rotations with smaller amplitude observed only for very high $c_A c_B$, i.e., here the mode of motion was quite different.) The amplitude reflects the maximum difference in interfacial tension caused by consumption of the surfactant during the chemical reaction.

We now summarize several results concerning the influence of geometric parameters in cylindrical containers:

(1) For fixed $r = 0.44$ and $c_A = c_B = 5 \times 10^{-2}$ M, the maximum lifetime was obtained in a vessel with $\phi = 24$ mm. It decreased for both smaller and larger ϕ ($T = 23°C$).

(2) For fixed $\phi = 19$ mm and $c_A = c_B = 10^{-2}$ M the lifetime increased with r in the range $0.3 < r < 1.0$ ($T = 24°C$).

(3) For $\phi = 19$ mm, $c_A = c_B = 8 \times 10^{-3}$ M and $T = 18°C$ there was one wave with maximum amplitude of 7 mm, independently of r; at $T = 20°C$, the number of waves was 2 (π-wave in Fig. 6) for $r < 0.3$ and 1 (2π-wave) for $r > 0.3$. The amplitude became smaller for $r < 0.8$ and then remained nearly constant ($h = 5.5$ mm) for $r < 0.6$.

(4) For $\phi = 19$ mm, $c_A = c_B = 2 \times 10^{-2}$ M and $T = 20°C$ the amplitude and the number of waves changed drastically at a critical value $r = 0.63$: for $r < 0.63$ $h = 3.5$ mm, $n = 2$; for $r > 0.63$ $h = 9$ mm, $n = 1$. Similarly, for $\phi = 19$ mm, $c_A = c_B = 5 \times 10^{-2}$ M and $T = 24°C$ we found $r = 0.75$ to be critical: for $r < 0.75$ $n = 2$; for $r > 0.75$ $n = 1$. This emphasizes the tendency that h decreases and n increases with decreasing r.

(5) The direction of motion changes occasionally from clockwise to anticlockwise and vice versa (seen from top). This happens mostly at a later stage of an experiment together with a change of the number n of waves. Direction and wave shape are correlated. Sometimes both directions are produced simultaneously and a source and a sink are formed. Although clockwise rotation was observed slightly more often in these experiments, there is no clear indication of any influence of Corioli's forces.

3.3 Temporal changes of interfacial motion

3.3.1 Qualitative behavior

An example for temporal evolution was already given in Fig. 7 in terms of potential difference. Due to closed conditions the gradual depletion of the reacting compounds necessarily leads to changes of motion which can be roughly devided into an induction, an intermediate, and a break-down phase. In one example (see (9)) first oscillations built up at the wall of a beaker, then about 3 waves rotated along the wall with constant velocity. Later this number decreased stepwise down to one, showing at each step a short period of transient behavior with fluctuating number

of waves. This decrease was first accompanied by an increase then by a decrease of the amplitude, until the wave motion vanished completely. As a general trend the number of waves decreases towards the end of an experiment and the profiles become more symmetric and smoother in time. The details of these trends depend, of course, on the particular region in the phase diagram.

As a further example we show in Fig. 13 typical changes in the rotation frequency of a wave, ω. In the upper graph (symbol □) we detect a slow modulation of ω around an average value of 1.8 s^{-1}, corresponding to a velocity $v = 9$ cm/s. This means that a low frequency is superimposed on the fast periodic motion (double periodicity). At 15 min the motion stops suddenly. In the second experiment with lower concentrations (symbol ●) such a double periodicity is only barely detectable, but the velocity decreases monotonically with time. At still lower concentrations (symbol ○) the wave rotation starts only after an oscillatory induction period of 4 min. Then its rotation frequency of initially 0.5 s^{-1} (velocity 3 cm/s) decreases also monotonically. In both latter cases the motion loses its activity gradually and vanishes after 15 min.

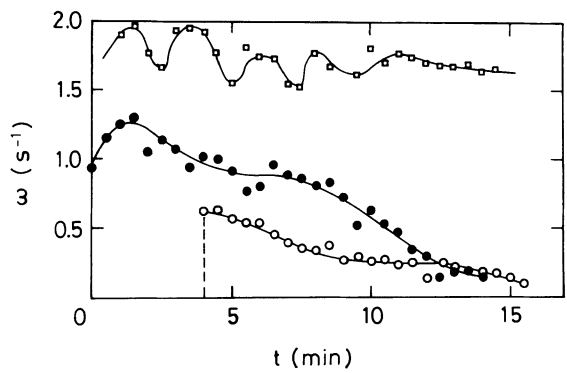

Fig. 13. Rotation frequency, ω, of a wave in a cylindrical vessel ($\phi = 16$ mm, $r = 0.625$) as a function of time. Initial concentrations: (□) $c_A = 8 \times 10^{-3}$ M, $c_B = 3 \times 10^{-2}$ M; (●) $c_A = 2 \times 10^{-3}$ M, $c_B = 8 \times 10^{-3}$ M; (○) $c_A = 5 \times 10^{-4}$ M, $c_B = 10^{-3}$ M.

3.3.2 Evolution under systematic variation of concentrations

A more comprehensive picture of the temporal evolution was achieved by observing the changes of interfacial motion under systematic variation of initial concentration combinations, as follows:

(1) c_A fixed at 5×10^{-3} M and 10^{-3} M, c_B varied (Figs. 14a and b, respectively);

(2) c_B fixed at 2×10^{-2} M, c_A varied (Fig. 14c);

(3) c_A and c_B varied under the condition $c_A = c_A$ (Fig. 14d).

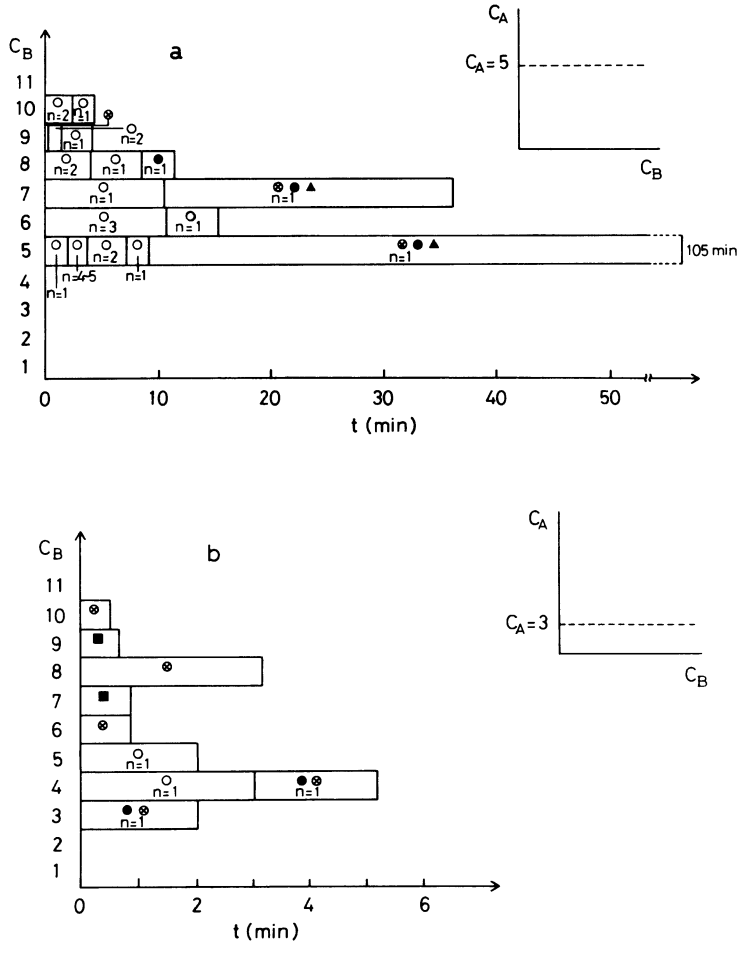

Fig. 14

The results for the first case ($c_A = 5 \times 10^{-3}$) are shown in Fig. 14a. As already seen in the phase diagram (Fig. 11) no macroscopic motion was observed for $c_B < 5 \times 10^{-3}$ M and the maximum lifetime was found at $c_A = c_B$. The different types of motion are indicated by different symbols specified in the caption. In general, the number n of waves decreases from several to one, and the lifetime of this wave is largest (e.g. up to 100 min for $c_A = c_B$), although it may be unsteady and sometimes intermittent. The initial state for $c_A = c_B = 5 \times 10^{-3}$ M with 4 to 5 waves is not stable and decays soon. It appears to be a regime of transition between stable motions. Figure 14b illustrates the aspects of the motion for $c_A = 10^{-3}$ M. The lifetime for

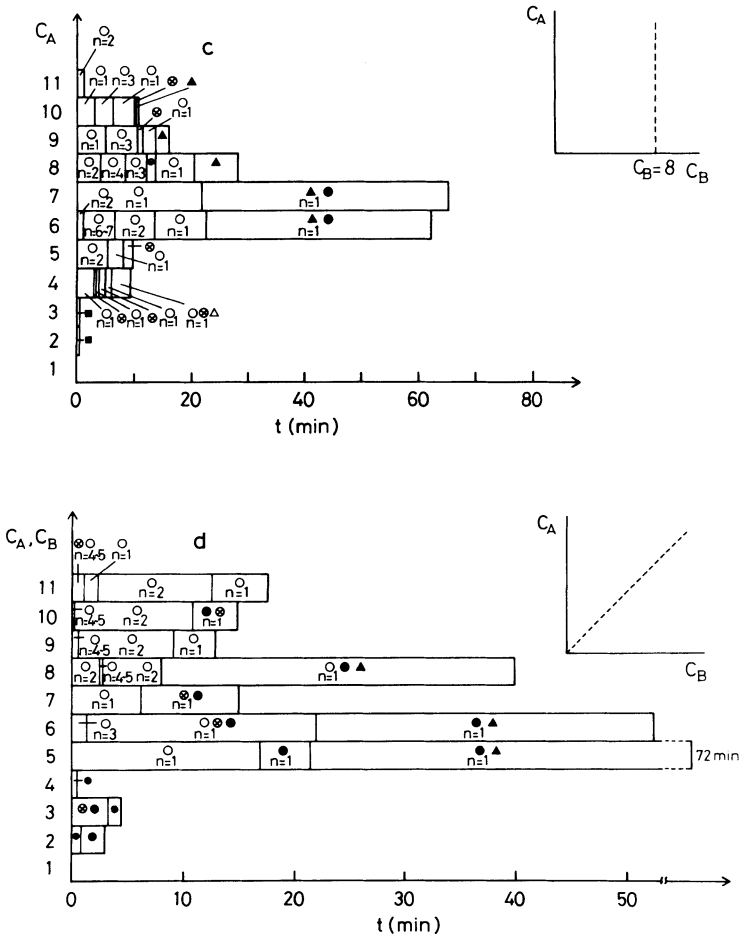

Fig. 14. Temporal changes of modes of interfacial motion in a cylindrical vessel ($\phi = 19$ mm, $r = 0.44$, $T = 22$–23°C). Choice of c_A and c_B (as indicated in the inserts): (a) $c_A = 5 \times 10^{-3}$ M, c_B varied; (b) $c_A = 10^{-3}$ M, c_B varied; (c) c_A varied, $c_B = 2 \times 10^{-2}$ M; (d) $c_A = c_B$, both varied. On the ordinates, the selected concentrations are labeled with numbers: $1 = 10^{-4}$ M, $2 = 5 \times 10^{-4}$ M, $3 = 10^{-3}$ M, $4 = 2 \times 10^{-3}$ M, $5 = 5 \times 10^{-3}$ M, $6 = 8 \times 10^{-3}$ M, $7 = 10^{-2}$ M, $8 = 2 \times 10^{-2}$ M, $9 = 3 \times 10^{-2}$ M, $10 = 5 \times 10^{-2}$ M, $11 = 10^{-1}$ M. In each section of the horizontal bars the number of waves (n) and the modes of motion are specified: steady rotation (○), unsteady rotation (●), source-to-sink propagation (Δ), irregular non-periodic oscillations with small amplitude (■), oscillatory motion without propagation (⊗), intermittency between rotational and oscillatory motion (▲).

these combinations was quite short ($\tau \leq 6$ min), and except for $c_B = 5 \times 10^{-3}$ M and 2×10^{-3} M no propagation but only interfacial oscillation appeared.

In Fig. 14c ($c_B = 2 \times 10^{-2}$ M constant) combinations close to the boundary line

in the phase diagram were realized (Fig. 11). Each of the bars shows details of a quite complex motion. Experiments 6 to 8 on the ordinate lie in the area of transitions between regions I, II, III, and IV and, therefore, the number of waves changes frequently, e.g., from $n = 2$ (not very stable) to $n = 6$ or 7 (of the incommensurate wave type, cf. Fig. 6d) to $n = 2$ to $n = 1$ (stable), also source-to-sink type propagation may occur (cf. Fig. 6e). For number 8 on the ordinate, the wave motion with successively $n = 2$, $n = 4$, $n = 3$ stops at $t = 15$ min and changes into oscillations. Remarkably, after about 2 min stable rotation with $n = 1$ starts again. When changing c_A along this route, we frequently encounter such oscillations.

Fig. 14d shows the dynamic behavior along the route $c_A = c_B$. In part, it corresponds to the boundary between regions with and regions without macroscopic motion (see phase diagram). Therefore, since small variations of initial conditions such as concentrations or temperature can result in large differences in behavior, only qualitative features but not the detailed aspects are reproducible.

3.4 Quantitative description of wave profiles

The properties of the interfacial waves were further studied by analyzing the shape of their profiles. For this purpose annular containers were used in which clearer wave shapes and more active motions are obtained. In Fig. 15a typical wave profile and its change in time were copied from a television screen. During the first minutes, the shape is symmetric and triangular ($t = 3$ min), later both the rising and the decaying slopes change to a more exponential type shape ($t = 13$ min) which becomes more pronounced after 20 min. The velocity remains almost constant (changing only slightly from 7.5 to 8 cm/s).

The upward movement indicates that the reaction reduces the concentration of surfactant at the interface, i.e., the tension γ_A increases and the interface is lifted up

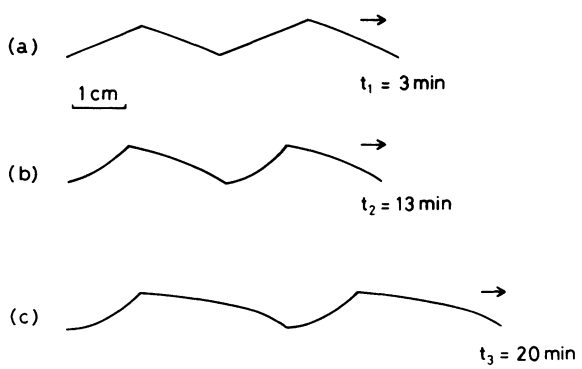

Fig. 15. Wave profiles in an annular container ($\phi_1 = 50.3$ mm, $\phi_2 = 45.1$ mm) with $c_A = c_B = 2 \times 10^{-2}$ M, copied from a TV monitor (without corrections). Time after start of experiment: (a) 3 min, (b) 13 min, and (c) 20 min. Wave velocities: (a) 7.5 cm/s, (b, c) 8 cm/s.

towards the aqueous phase. By contrast, during the downward movement, the processes are controlled by diffusion carrying new reactant from the bulk to the phase boundary. In a qualitative way, one can state that in the profile (a) the time constant and saturation value for the reaction and the diffusion controlled steps are both large. In profile (b) and more so in profile (c) the time constants of the rising slope have decreased substantially. For the decaying tail a significant change takes place only from (a) to (b), but no more at a later time.

These qualitative features were confirmed in an experiment with similar wave shape that was reconstructed quantitatively from a time series (see Subsection 2.3). In Fig. 16 the profiles $h(z)$ in a moving frame (variable z) could be fitted by exponential functions. For the lower of the two shown cases these are:

$$h(z) = 0.81\Big(1 - \exp\big(-0.97(z - \xi)\big)\Big)$$

for the leading slope and

$$h(z) = 0.78\exp(-1.82z)$$

for the decaying tail, where $z = x - vt$ with x denoting the position and v the velocity of the waves and $\xi = 4.7$ cm. For the upper profile, which was obtained at an earlier time, the decay function is the same but the leading slope rises faster and is shorter ($\xi = 4.1$ cm). Thus, the analyzed example suggests that the phenomenon is related to the relaxation type oscillations as known from other chemical oscillators (3).

In Fig. 17 the profiles of waves are drawn that split and recombine (without

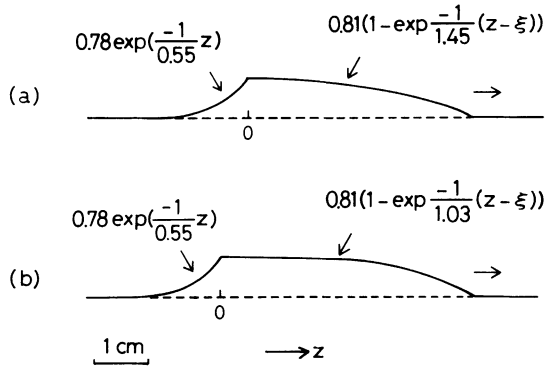

Fig. 16. Wave profiles in an annular container ($\phi_1 = 80$ mm, $\phi_2 = 75$ mm) with $c_A = c_B = 5 \times 10^{-3}$ M at $T = 20$°C. Time after start of experiment: (a) 5 min and (b) 25 min. Wave velocities: (a) 2.6 cm/s, (b) 3.5 cm/s. In a moving frame (variable z) the profiles are represented by exponential functions G (with $\xi = 4.1$ cm (a) and $\xi = 4.7$ cm (b)).

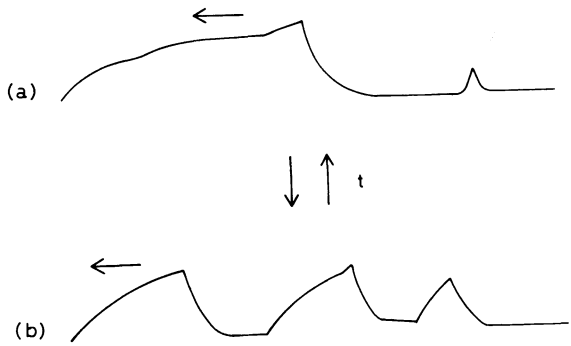

Fig. 17. Profiles of a pattern in which waves split and recombine, as observed in an annulus ($\phi_1 = 80$ mm, $\phi_2 = 70$ mm) with $c_A = c_B = 5 \times 10^{-3}$ M at $T = 23$°C. Times of observation: (a) start of the experiment and (b) 3 min later. Wave velocities: (a) 9.4 cm/s, (b) 7.3 cm/s.

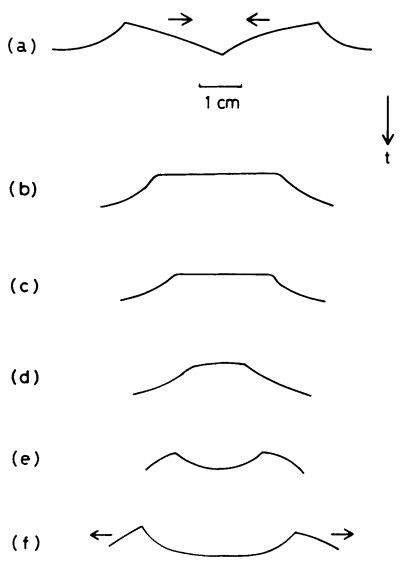

Fig. 18. Wave collision in an annulus ($\phi_1 = 50.3$ mm, $\phi_2 = 45.1$ mm) with $c_A = c_B = 5 \times 10^{-3}$ M. Wave velocity is 10 cm/s. Times after start of experiment: (a) 0 s, (b) 0.1 s, (c) 0.15 s, (d) 0.2 s, (e) 0.75 s, (f) 1.0 s. Arrows indicate direction of propagation.

correction). At the beginning of the reaction, one flat and large wave with $h_{max} = 1.4$ cm and a small triangular wave rotate steadily along the glass wall with $v = 9.4$ cm/s (Fig. 17a). The small wave may be regarded as a damped successor of the large one. For several times, the large wave then splits into smaller waves and recombines

again and therefore it may itself be regarded as superposition of several smaller waves. After 3 min a final splitting into 3 waves of similar size and shape takes place which further on rotate with $v = 7.3$ cm/s (Fig. 17b).

Figure 18 depicts a scenario of wave collision recorded in a system with $c_A = c_B = 5 \times 10^{-3}$ M. Within 1 s two waves pass through each other and emerge in only slightly modified form. In this collision process the waves behave like common solitons. Two other types of wave interaction have been observed: waves with large amplitude absorb waves with small amplitude upon collision; two colliding waves with equal amplitude may annihilate each other.

4. Discussion

4.1 Summarizing comments

A large variety of spatiotemporal structures occurring at a liquid-liquid interface has been described in terms of visual observation, electropotential measurements, construction of a phase diagram, and measurement of wave profiles. The phase diagram can be divided into 5 regions: (1) regions I and II where basically four different modes of macroscopic steady motion are observed, i.e., solitons, rotating multiple waves, oscillations, and chaotic motions; (2) region III where a periodic stretching motion appears; (3) region IV where the motion is unsteady and intermittent; and (4) the remaining regions where one observes no macroscopic motion but only formation of a microemulsion with microscopic irregular dynamics. The lifetime and the activity of motion in this closed system are largest, if the initial solute concentrations are equal, and increase over a wide range with the concentration product. During evolution, sharp transitions between different dynamic regimes occur. The local time course of the motion can be described more quantitatively by the difference of electrochemical potential. The dynamical behavior is not only caused by changes in interfacial tension but changes in the electrical conditions (ionic concentrations) in the bulk and its influence on the interface.

4.2 Mechanistic aspects

As mentioned previously, surface waves on a water column in a beaker may show properties that are similar to those of the currently investigated system (19, 20). This so-called bell mode instability, which results in macroscopic elastic wavelike surface deformation, is caused by nonlinear interaction between the modes of water waves and an externally applied periodic force with a much higher frequency than that of the waves. In this case, when the frequency of the external driving force deviates from a certain resonance frequency, wave propagation along the glass wall occurs. This phenomenon has been studied in several theoretical papers. The basic mechanism of the interfacial system under consideration would be almost the same, if the chemical reaction processes were regarded as equivalent to the external periodic driving force. However, no explanation in terms of such a

direct analogy has been put forward yet.

Since the phenomenon under consideration is driven by the chemical reaction through the interface (adsorption and desorption), the dynamic features must be largely influenced by the reaction kinetics, by transport processes such as diffusion and convection, as well as by the influence of concentration variations on the physical boundary conditions, in particular on the forces acting at the interfaces.

From the phase diagram in Fig. 11 and spectral analysis of the electrochemical potential traces in Figs. 8 to 10 we learn that in region I of the diagram periodic rotation prevails, but that in region II a noisy component is superimposed. For the highest concentrations in region II the nonperiodic irregular motion even dominates and interfacial turbulence can be clearly observed. Accordingly, different mechanisms appear to contribute to the wavelike displacements, all of which are based on the variation of interfacial tensions: The interfacial turbulence is caused by the Marangoni instability (16, 17). It leads to hydrodynamic transport of the ions from the bulk to the interface and usually remains on a small scale. The major reason for the large scale displacements ($\approx$10 mm) is the capillary effect: the interface is lifted up or pulled down by the changes of interfacial tension between oil and water. This depends largely on the difference and does not involve convective flow. In addition, the dynamical wetting induces changes of the contact angle and thus may contribute to the large scale displacements. It is, however, restricted to areas near the solid boundary. While capillary effect and wetting dominate in region I, the interfacial random convection becomes noticeable only in region II. For the highest concentrations used, it has considerable influence and the wavelike motion is then strongly coupled with pronounced interfacial turbulence.

Evidence has been presented about the important role of the concentration product as a driving force of the phenomenon: the larger $c_A c_B$ the faster and more pronounced the motion (Fig. 12). The fact that the maximum rotation frequency is a linear function of the logarithm of $c_A c_B$ suggests that the rotation velocity is closely connected to the chemical reaction kinetics. By contrast, the maximum amplitude is essentially independent of this product, because it is mainly determined by differences in interfacial tension, thus by the magnitude of the concentration change during the reaction, rather than by the reaction velocity. It should depend on the resulting concentration difference which we assume to be determined by threshold values of $c_A c_B$ at which the reaction is turned on and off (see below).

Among the observed waves, we consider here those having relaxation type profiles. The exponential shapes shown in Figs. 15 and 16 and the arguments for the role of reaction, diffusion and driving force present a basis for preliminary modelling. The main processes for the formation of the waveform are controlled by reaction for the rising slope and by diffusion for the decaying slope. Apparently, the chemical processes at the interface lead often to such relaxation type oscillations as they occur in other chemical nonequilibrium systems. As a first step, the phenomenon of wave propagation could be interpreted as a change of phase across a set of spatially distributed relaxation type oscillators. But this picture does not lead very

far as to understand the nature of the spatial coupling of neighboring volume elements.

4.3 A simple model

Figure 19 shows schematically a possible explanation for the formation of oscillatory behavior at the interface. The role of the capillary effect is emphasized, any change of the contact angle is neglected ($\alpha = 90°$) and convection is disregarded: Suppose that the chemical reaction starts and stops at two different threshold values of the concentration product $K (= c_A c_B)$, $K_c\uparrow$ and $K_c\downarrow$ ($K_c\uparrow > K_c\downarrow$), respectively, and that the state of the system is metastable at any value between these thresholds. We start from the top of a wave. When ions are transported to the interface by diffusion, the interfacial tension decreases, because more surfactant molecules become available to form a monolayer. As a consequence of the capillary effect the interface sinks down in the gravitational field. The increase of ions leads to the reaction start at $K > K_c\uparrow$, ions at the interface are consumed so that the difference of interfacial tensions increases leading to an increase of the wave amplitude. The reaction continues until $K < K_c\downarrow$ with a time scale faster than that of diffusion. After the reaction has stopped due to depletion of available reactant, diffusion comes into play again, thus allowing the ion concentration to be newly built up at the interface so that repetition of the sequence can occur. In Fig. 19 the time course of this repetitive competition between the reaction and the diffusion controlled steps is depicted. Wave propagation could be introduced simply by a propagating phase shift between local oscillators, but this includes no assumption about the nature of the spatial coupling (4). Evidently, a more sophisticated mechanism for spatial coupling leading to propagation phenomena has to be implemented.

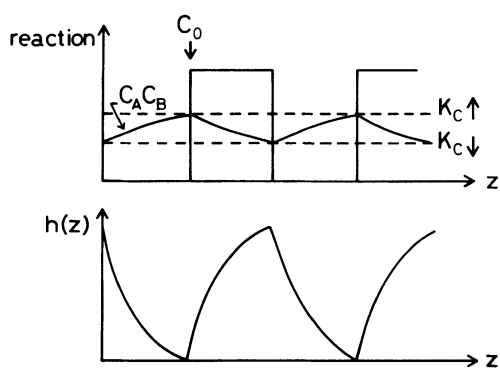

Fig. 19. Schematic drawing of a relaxation-type oscillation, based on a phenomenological model (see text). $h(z)$: wave amplitude with $z = \omega t$ (ω = rotation frequency), $K_c\uparrow$: threshold for start of reaction, $K_c\downarrow$: threshold for end of reaction.

Also the bell mode instability, caused by the nonlinear coupling between fast modes (the reaction as the external driving force) and slow modes (the macroscopic surface wave), may play an important role for a complete mechanism. When interfacial turbulence due to the Marangoni effect is only weakly developed, the chemical reaction probably enhances more and more the deformations and nonlinear coupling both to the amplitude and to the turbulent flow component takes place.

5. Conclusions

The investigated temporal and spatial structures forming at an oil-water interface are driven by a chemical reaction coupled with transport processes and hydrodynamic convection. The macroscopic motions are highly nonlinear and occur under far from equilibrium conditions. There are mainly two mechanisms involved: one is convection due to the Marangoni instability, that is hydrodynamic transport arises from gradients in interfacial tension and induces turbulent behavior, the other is the capillary effect, meaning that interfacial tension differences lead to vertical displacements of the interface. Furthermore, changes of the contact angle have to be considered. Which of these plays a more important role depends on the conditions of the experiment. The first mechanism probably dominates for relatively high, the second for relatively low solute concentrations.

It may be necessary to include an additional mode of deformation, namely the elastic one, e.g., for thoroughly understanding periodic isotropic stretching motion (see Fig. 5g) which resembles the typical bell mode with the wavenumber $k = 0$. Because of the phenomenological similarities between our reactive system and the bell mode instability it will be useful to consider such an elastic hydrodynamic instability in order to obtain further ideas for the appropriate mechanism.

The present system is very complicated, because four initial reactants, an unknown number of relevant intermediates, at least three hydrodynamic components, and electrochemical aspects are involved. Therefore, a quantitative discussion was not yet performed. The results call for modelling efforts in which the nonlinear behavior is simplified by reduction to a small number of most relevant properties. The interfacial system described here, which is easily accessible to further experimentation, certainly offers interesting aspects for exploring bifurcation and nonlinear propagation phenomena under nonequilibrium conditions. Such efforts are under way on the basis of a refined set of experimental data (22).

Acknowledgement

S. C. M. thanks for a research fellowship from the Japanese Society for the Promotion of Science (JSPS).

REFERENCES

(1) Chandrasekhar, S., Hydrodynamic and Hydromagnetic Stability, Clarendon Press, Oxford, 1961.
(2) Swinney, H. L. and Gollub, J. P. (eds.), Hydrodynamic Instabilities and the Transition to Turbulence, 2nd edition (Springer-Verlag, Berlin Heidelberg, 1986).
(3) Field, R. J. and Burger, M. (eds.), Oscillations and Traveling Waves in Chemical Systems (Wiley Interscience, New York, 1985).
(4) Ross, J., Muller, S. C., and Vidal, C. (1988), Science, **240**, 460.
(5) Glansdorff, P. and Prigogine, I., Thermodynamic Theory of Structure, Stability and Fluctuations (Wiley Interscience, New York, 1971).
(6) Dupeyrat, M. and Michel, J. (1971), J. Exp. Suppl., **18**, 269
(7) Nakache, E., Dupeyrat, M., and Vignes-Adler, M. (1983), Experimental and theoretical study of an interfacial instability at some oil-water interfaces involving a surface-active agent, J. Colloid Interf. Sci., **94**, 187.
(7) Nakache, E., Dupeyrat, M., and Vignes-Adler, M. (1984), The contribution of chemistry to new Marangoni mass-transfer instabilities at the oil/water interface, Faraday Discuss. Chem. Soc., **77**, 189–196.
(8) Yoshikawa, K., Maeda, S., and Kawakami, H. (1988), Various oscillatory regimes and bifurcations in a dynamical chemical system at an interface, Ferroelectrics, **77**, 281–298.
(9) Kai, S. and Müller, S. C. (1985), Spatial and temporal macroscopic structures in chemical reaction systems, Sci. Form, **1**, 9–39.
(10) Kai, S., Ooishi, E., and Imasaki, M. (1985), Experimental study of nonlinear waves on interface between two liquid phases with chemical reaction, J. Phys. Soc. Jpn., **54**, 1274–1281.
(11) Sackmann, E., in Temporal Order, edited by Rensing, L. and Jaeger, N. I., p. 153, Springer-Verlag, Berlin, 1984.
(12) Sternling, C. V. and Scriven, L. E. (1959), A. I. Ch. E. J., **5**, 514.
(13) Scott, A. C. (1979), Sine-Gordon breather dynamics, Phys. Scripta, **20**, 509–513.
(14) Fukuda, T. and Kotani, M. (1986), A numerical study of nonlinear diffusion equation governing surface deformation in the Marangoni convection, J. Phys. Soc. Jpn., **55**, 3857–3862.
(15) Takaki, R. and Sannomiya, K. (1989), Self-excited wave on an interface in a chemical reaction, Forma, **4**, 35–47.
(16) Scriven, L. E. and Sternling, C. V. (1960), Nature, **187**, 186.
(17) Sanfeld, A. and Steinchen, A. (1984), Motion induced by surface-chemical and electrochemical kinetics, Farad. Discuss. Chem. Soc., **77**, 1–11.
(18) Findenegg, G. H. and Loring, R. (1984), Fluid absorption up to the critical point. Experimental study of a wetting fluid/solid interface, J. Chem. Phys., **81**, 3270–3276.
(19) Mahony, J. J. and Smith, R. (1972), On a model representation for certain spatial resonance phenomena, J. Fluid Mech., **53**, 193–207.
(20) Huntley, I. (1977), Spatial resonance of a liquid-filled vibrating behavior, J. Fluid Mech., **80**, 81–97.
(21) Kai, S., Mori, T., Mutsumaru, M., and Muller, S. C. (1991), Physica, **D50**, 412–428.
(22) Kai, S., Miki, M., and Mori, T. (1991), Part II of this series in this book.